Applied Surface Science 499 (2020) 143989

Contents lists available at ScienceDirect

Applied Surface Science

journal homepage: www.elsevier.com/locate/apsusc

Full length article

Tribochemistry of TaN, TiAlN and TaAlN coatings under ambient atmosphere and high-vacuum sliding conditions

D. Dinesh Kumar[a,b,*], Revati Rani[c], Niranjan Kumar[c,**], Kalpataru Panda[d], A.M. Kamalan Kirubaharan[a], P. Kuppusami[a], R. Baskaran[b]

[a] Centre for Nanoscience and Nanotechnology, Sathyabama Institute of Science and Technology, Chennai 600119, Tamil Nadu, India
[b] Department of Physics, Academy of Maritime Education and Training, Chennai 603112, Tamil Nadu, India
[c] Materials Science Group, HBNI, Indira Gandhi Centre for Atomic Research, Kalpakkam 603 102, India
[d] Center for Nanomaterials and Chemical Reactions, Institute for Basic Science, Daejeon 305-701, Republic of Korea.

ARTICLE INFO

Keywords:
Chemical bonding
Microstructure
Friction and wear
Tribolayer
Tribochemistry.

ABSTRACT

Tribochemical analysis of monolithic TaN, TiAlN, and TaAlN coatings deposited by reactive magnetron sputtering onto 316LN stainless steel (SS) substrates are described. Tribology experiments were carried out in ambient atmospheric and high-vacuum sliding conditions to investigate the tribo-atmospheric dependent friction and wear characteristics of these coatings. The lower friction coefficient and improved wear-resistant properties were observed for TaN and TiAlN coatings in the humid atmosphere than in high-vacuum testing condition. Interestingly, lower friction and wear resistance properties of TaAlN coated SS are significantly enhanced in atmospheric as well as high-vacuum sliding conditions because of their highly dense and fine-grained microstructure with stable cubic B1 TaAlN phase. Energy dispersive X-ray spectroscopy elemental mapping and microfocused X-ray photoelectron spectroscopy were carried out on the wear tracks to explore the comprehensive tribo-environment dependent tribochemistry. Formations of alumina (Al_2O_3) rich tribolayer reduced the friction and enhanced the wear resistance of TaAlN/SS sample tested in atmospheric condition; whereas this coating is highly stable in the high-vacuum condition with higher wear resistance.

1. Introduction

Wear-resistant coatings are increasingly important in various industries including cutting tools, automobile, aircraft, and biomedical industries to protect the interacting solid surfaces. For this purpose, numerous combinations of nitride based ceramic coatings and coating architectures were developed [1–3]. Incorporation of Al in binary ceramic nitride phases are gaining much interest concerning many industrial needs because of their improved mechanical, tribological, oxidation resistance and corrosion resistance properties especially in high-temperature conditions [4–6]. During high-temperature operations, formation of aluminum oxide (Al_2O_3) layers on the coatings surface effectively prevents the further diffusion of oxygen towards the coating interior [6,7]. Therefore, coatings of such materials like TiAlN and CrAlN are commercially used as protective tribological coatings on several sliding mechanical systems in harsh environments [6,8]. Still, there is an on-going demand for developing advanced materials with enhanced protection efficiency for better longevity and high load bearing capability [9]. Tantalum-based hard coatings are also widely studied in recent years for the wear resistant applications due to their advanced properties [10,11]. Recent reports imply that the addition of a small fraction of Ta within the TiAlN ternary coatings is significantly improved the hardness and phase stability under extreme temperature [12,13]. In these structures, the substitution of Ti^{4+} by Ta^{5+} in rutile TiO_2 phase formed at elevated temperature (> 800 °C) in TiAlN coating which reduces the number of oxygen vacancies and promotes the Al_2O_3 formation [14]. Similar enhancement of oxidation resistance is recently achieved by Chen et al. [15] for the TaN coatings by forming the solid solutions of Al in TaN at high-temperature. However, the recent studies have been majorly focused on the high-temperature oxidation tests of TaAlN coatings deposited using various PVD techniques [15–17]. Till now, limited studies have been carried out to understand the friction and wear characteristics of TaAlN coatings for tribological applications. Schalk et al. [18] studied high-temperature tribological properties of

* Correspondence to: D.D. Kumar, Centre for Nanoscience and Nanotechnology, Sathyabama Institute of Science and Technology, Chennai 600119, Tamil Nadu, India.
** Corresponding author.
E-mail addresses: ddinesh.tribology@gmail.com (D.D. Kumar), phystribology@gmail.com (N. Kumar).

https://doi.org/10.1016/j.apsusc.2019.143989
Received 16 May 2019; Received in revised form 6 September 2019; Accepted 11 September 2019
Available online 12 September 2019
0169-4332/

$Ta_{1-X}Al_XN$ coating with varying the Al concentration. Similarly, Hao et al. [19] reported that the incorporation of Mo into the TaAlN coating would enhance the tribological properties. On the other hand, tribochemistry plays a key role in determining the friction and wear characteristics of coatings, since it leads to change in chemical and physicochemical properties of the coatings [20–22]. Bobzin et al. [23] observed that the oxidized tribochemical particles of $Cr_{1-x}Al_xN$ are responsible for microcutting of coating which leads to the higher wear. Dante and Kajdas [24] reported that the tribochemical products of Si_3N_4 were formed tribofilms at the sliding interface which leads to decreasing contact stress and protects the Si_3N_4 surface from further wear. Moreover, lower friction was achieved by Du et al. [25] for the TaC_xN_y films owing to the tribochemical induced formation of graphitic clusters. Similarly, several tribochemistry studies have been conducted for different hard coatings under dry as well as boundary lubricated conditions [26–28]. Therefore, comprehensive tribochemical analysis on the tribolayer of sliding interfaces is important for understanding the tribological properties of the coatings. Moreover, the evaluation of tribo-atmosphere dependent tribological properties is also required to understand the friction and wear characteristics of ternary nitride coatings for the purpose of solid lubricants.

In this work, we have carried out detailed comparative studies on the tribological properties of TaN, TiAlN, and TaAlN coatings in atmospheric and high-vacuum tribo-conditions to understand the friction and wear behaviour with respect to changes in sliding conditions. For this purpose, the TaN, TiAlN, and TaAlN coatings have been deposited on 316LN SS substrates using reactive DC magnetron sputtering technique under optimized process conditions. The detailed microstructure, chemical bonding and tribological properties of these coatings were studied using various characterization techniques. The energy dispersive X-ray spectroscopy (EDAX) and X-ray photoelectron spectroscopy (XPS) have been used for the analysis of tribo-chemical changes and understanding the governing factors of friction and wear behavior under selected tribological conditions.

2. Experimental details

2.1. Coatings deposition

The coatings were deposited on the surface polished 316LN SS substrates with the dimensions of 20 × 20 × 1.5 mm using reactive DC magnetron sputtering (Plassys, MP300, France) technique. High-purity materials (99.995%) of Ta, TiAl (50:50) and TaAl (50:50) have been used as target materials. The target-substrate distance was maintained at 75 mm. Prior to deposition, the chamber was evacuated up to the base pressure of 2×10^{-6} mbar using rotary and turbomolecular pumps. During the deposition, the chamber was partially filled by the nitrogen gas with the pre-optimized flow rates of 5 and 7 sccm for TaN, and TiAlN, TaAlN coatings, respectively along with the Ar gas flow rate of 15 sccm. The total working pressure and the substrate temperature were maintained about 2×10^{-3} mbar and 300 °C, respectively. To remove the surface contaminations, all the target surfaces were sputter cleaned for 5 min with the sputter power of 100 W. All the depositions were carried out for 1 h with the target power of 150 W. Metallic Ta and Ti interlayers of ~ 150 nm have been deposited prior to the respective coatings to improve the adhesion between the substrates and coatings.

2.2. Coatings characterization

Chemical bonding of coatings was analyzed by XPS technique (Sigma probe-Thermo VG scientific, USA) using Al Kα radiation (E = 1486.6 eV) with the energy resolution of 0.47 eV in ultra-high vacuum (UHV) of 1.3×10^{-10} mbar. The structural properties of the coatings were analyzed using X-ray diffraction (XRD) technique, Miniflex II, Rigaku, Japan with the step size of 0.02° using Cu Kα radiation (wavelength, λ = 1.5406 Å). Surface morphologies and topographies of the coatings were observed using field emission scanning electron microscopy (FE-SEM, Carl Zeiss Supra 55, Germany) and atomic force microscopy (AFM, NT-MDT, Ireland) techniques, respectively. The tribological properties of all the coatings were analyzed using Anton Paar tribometer (Switzerland) under atmospheric and high-vacuum sliding conditions. The 100Cr6 SS balls with 6 mm diameter were used as sliding contact bodies with the sliding speed of 100 rpm (linear speed:1.04 cm/s). The high-vacuum test was conducted at the chamber pressure of 3×10^{-6} mbar. The wear track width and depth was estimated using Dektak stylus profilometer (Bruker, USA). The wear track morphology of all the coatings after tribology measurements was analyzed using FE-SEM technique. The tribochemistry of the wear surface of all the tested coatings was investigated using EDAX elemental mapping and micro-focused XPS with the spatial resolution of 100 μm.

3. Results and discussion

3.1. Chemical bonding analysis

Chemical bonding nature of as-deposited coatings was analyzed using XPS technique. The survey spectrum of these samples indicated that all the primary elements are presented in their respective coatings which are shown in Fig. S1 (see supplementary data). The core level high-resolution XPS analyses of every element were carried out to analyze the chemical bonding nature (Figs. 1-3). Table 1 shows the quantitative chemical compositions of as-deposited TaN, TiAlN and TaAlN coatings. The resultant spectra of TaN coating (Fig. 1a-c) indicate Ta and N as major elements along with the O. The deconvoluted Ta 4f spectrum (Fig. 1(a)) indicates two major doublet peaks at ~22.8 eV ($4f_{7/2}$) and ~24.6 eV ($4f_{5/2}$) corresponding to the formation of covalent bonding between Ta and N due to the spin-orbit coupling energy 1.9 eV [29]. It is confirmed that these peaks shifted to higher binding energies as compared to the reported binding energy of metallic Ta (~21.7 eV) [22]. Moreover, Ta—O—N and Ta—O boding were noticed from their respective peak positions at ~25.8 eV and ~27.4 eV, as shown in Fig. 1(a) [29]. Similarly, N 1s spectra (Fig. 1b) can be deconvoluted into two peaks which include high-intensity peak positioned at ~397.1 eV and a shake-up-peak at ~396.1 eV corresponding to the covalent bonding of Ta—O—N and Ta—N, respectively [22,29]. In addition, a broad Ta $4p_{3/2}$ component peak is overlapped with N 1s peak at the binding energy of 400–405 eV (Fig. 1b). The Ta $4p_{1/2}$ is difficult to obtain in N 1s spectra because of its asymmetric nature. Moreover, the signature of Ta—O—N and Ta—O bonding were observed in the O 1s spectra (Fig. 1c) with their respective binding energies of 530.1 eV and 531.5 eV, respectively [30]. These oxides are merely surface oxides (Ta_2O_5) which could be due to the large difference in electronegativity of Ta with oxygen from the atmosphere and reactive nitrogen gas used for the TaN deposition [31].

Fig. 2a-d shows the high-resolution XPS spectra of Ti 2p, Al 2p, N 1s and O 1s core levels of TiAlN coating. The Ti 2p spectra can be deconvoluted into several peaks as illustrated in Fig. 2a. Amongst them, spin-orbit doublets of Ti $2p_{3/2}$ consists of three major peaks at ~455.2 eV, ~456.5 eV and ~458.2 eV are attributed to the binding energies of Ti—Al—N, Ti—O—N, and Ti—O bonding, respectively reveals the strong affinity of Ti with N. The spin doublet Ti $2p_{1/2}$ and the shake-up peaks in the binding energies between 460 and 465 eV representing the bonding of oxide phases (i.e. TiO_2) [32,33]. The oxygen reactivity in TiO_2 arises due to the higher affinity of O atoms located in the Ti interstitial sites [34]. The Al 2p spectra in Fig. 2b included two major deconvoluted peaks which are associated to the Ti—Al—N (73.2 eV) and Al—N (74.4 eV) corresponding to the Al $2p_{3/2}$ and Al $2p_{1/2}$ spin doublets [32]. Similarly, the N 1 s spectra can be fitted with several Gaussian peaks as illustrated in Fig. 1c. These peaks might be due to the well-resolved phases of Ti—Al—N (395.6 eV), Ti—N (396 eV), Ti—O—N (396.8 eV) and Al—N (397.9 eV). A broad shake-up satellite peak has

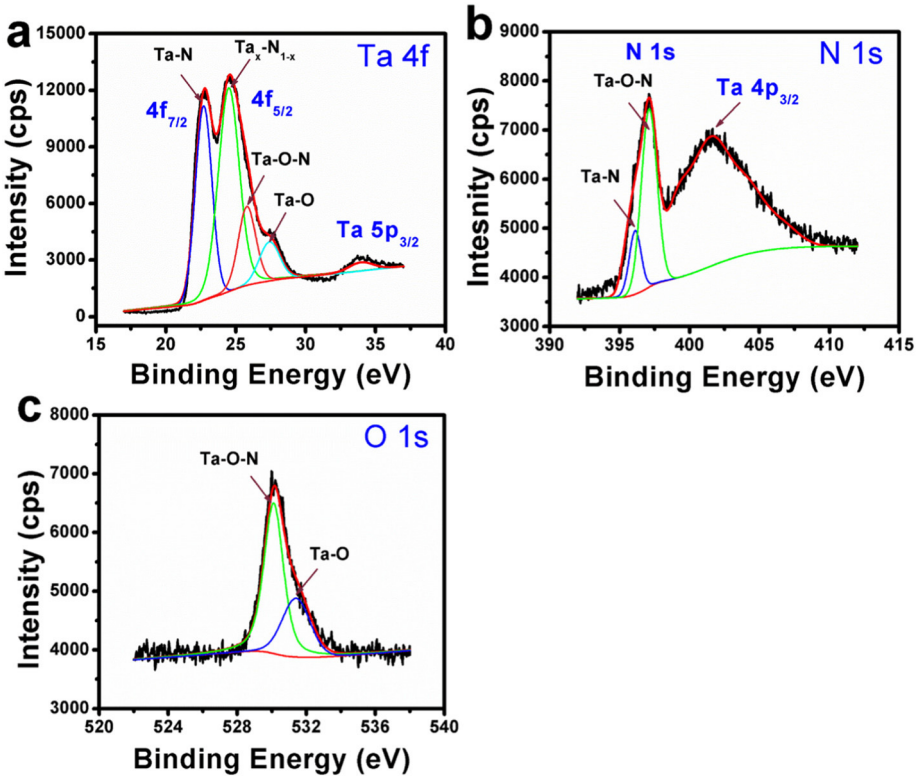

Fig. 1. High-resolution XPS spectra of TaN coating: (a) Ta 4f, (b) N 1s and (c) O 1s deconvoluted spectra.

also been observed at 399.4 eV is due to the N adsorption over the surface subsequently during the deposition process [32]. Moreover, the metal-oxides and oxynitride bonding are formed on the sample as demonstrated from the O 1s spectrum (Fig. 2d), associated to the TiO_2 (530.6 eV) and Al_2O_3 (532 eV) phases. Such surface oxides and oxynitride layers formed upon exposure of the sample to the atmosphere after deposition.

Fig. 3a-c illustrated the high-resolution XPS spectra of TaAlN coating components such as Ta 4f, Al 2p, N 1s, and O 1s. Two major spin doublets Ta $4f_{7/2}$ and Ta $4f_{5/2}$ and four minor deconvoluted

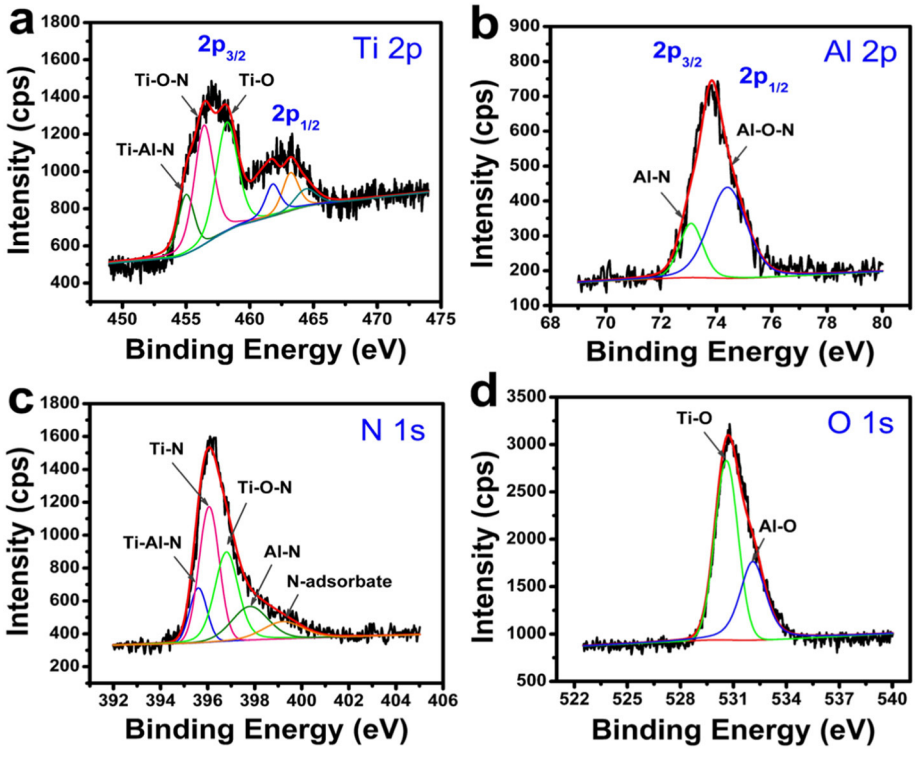

Fig. 2. High-resolution XPS spectra of TiAlN coating: (a) Ti 2p, (b) Al 2p, (c) N 1s and (d) O 1s deconvoluted spectra.

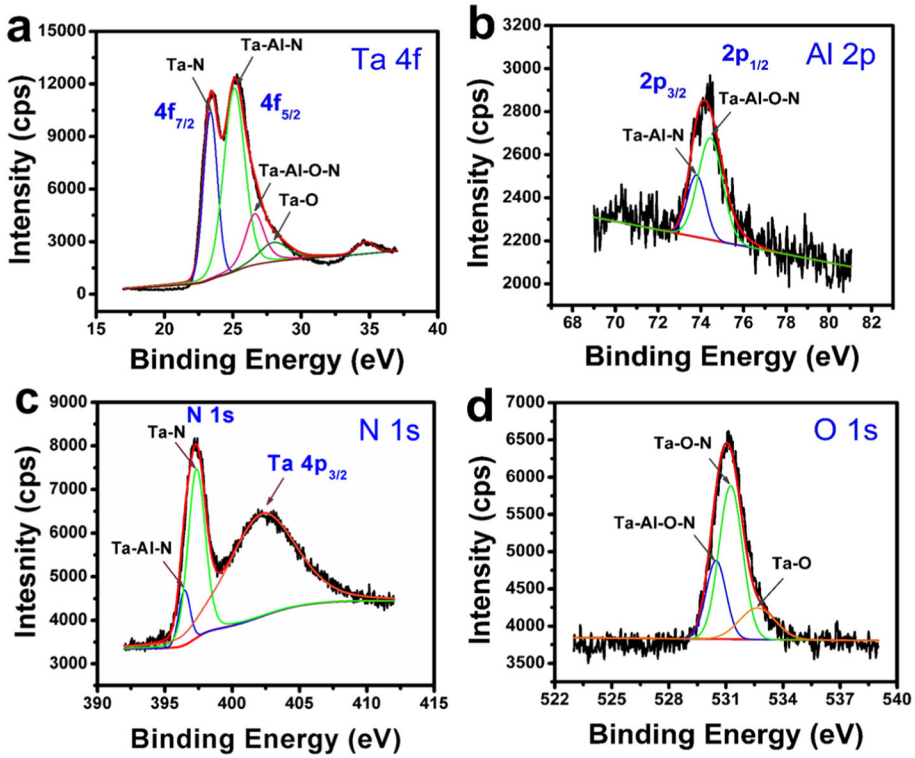

Fig. 3. High-resolution XPS spectra of TaAlN coating: (a) Ta 4f, (b) Al 2p, (c) N 1s and (d) O 1s deconvoluted spectra.

regions are ascribed to the several nitride phases of Ta−N (23.4 eV), Ta−Al−N (25.3 eV), and Ta−Al−O−N (26.5 eV). These binding energies are shifted to the higher side than that of TaN coating (Fig. 1a), which clearly depicts the co-sputtered Al is interstitially located into the TaN phase to form Ta−Al−N bonding [29,34]. The additional shake-up peak at 27.6 eV is owing to the Ta−O bonding (Ta_2O_5 phase). The Al 2p spectra show two spin states (i.e. $2p_{3/2}$ and $2p_{1/2}$) with the binding energies of 73.7 eV and 74.4 eV which could be attributed to the Ta−Al−N and Ta−Al−O−N phases, respectively as illustrated in Fig. 3b. Moreover, the formation of Ta−Al−O−N (396.4 eV) and Ta−N (397.3 eV) bonding along with Ta $4p_{3/2}$ (402.4 eV) were observed in the N 1s spectra (Fig. 3c) [35,36]. The signature of oxide phases are clearly revealed from the O 1s spectra (Fig. 3d) at the peak positions ~530.4 eV, 531.3 eV, and 532.6 eV which agree to the formation of Ta−Al−O−N, Ta−O−N, and Ta−O bonding, respectively.

3.2. Structural and surface analysis

Fig. 4 shows the XRD patterns of TaN, TiAlN, and TaAlN coatings deposited on 316LN SS substrates. The peaks of TaN coating (Fig. 4a) are well-matched with the face-centered cubic (fcc) TaN phase (JCPDS#49–1283) with the corresponding planes of (111), (200), (220), (311) and (222). The TaN phase formation results are in accordance with the XPS spectra (Fig. 1). The preferred orientation of (200) plane in TaN coating depends on the lowest energy which derived from the critical competition between surface and strain energies of (200) plane during the coating deposition at lower substrate temperature [37]. The lattice parameter of TaN phase was calculated using the 'Unit Cell Program' software [38] and found to be 4.315 Å. The obtained lattice parameter is lesser than the reported value (4.339 Å) indicating the presence of tensile stress in the coating. A peak positioned at 38.4° representing the formation of Ta_2N phase (JCPDS#26-0985) is due to the stress accumulation in the coating which can be controlled by increasing the substrate temperature or by annealing [39]. For TiAlN coating (Fig. 4b), the peak positioned at 37.7° corresponds to the (111) plane of cubic phase of TiAlN which is matched well with the previously reported data. The lattice parameter of the TiAlN coating is found to be 4.143 Å which is slightly lower than the reported value [40]. Owing to the lower substrate temperature and lattice distortions of Al substituted Ti atoms, less crystalline TiAlN is forming. In TiAlN lattice, larger sized Ti atoms in the TiN structure are substituted by smaller Al atoms [32]. That is the reason why the peaks of TiAlN coating slightly shifted from standard 2θ values. TiAlN coating showed tensile stress (lattice parameter is lesser than the bulk reported value) which is not common in nitride-based coatings. This is due to lower deposition temperature and lesser atomic peening effect during deposition [41]. In TaAlN coating, the formation of a highly intense sharp peak at 42.14° identified as solid solution of B1 TaAlN (200) phase with

Table 1
XPS and EDAX elemental composition of as-deposited TaN, TiAlN and TaAlN coatings.

TaN			TiAlN			TaAlN		
Elements	XPS (at.%)	EDAX (at.%)	Elements	XPS (at.%)	EDAX (at.%)	Elements	XPS (at.%)	EDAX (at.%)
Ta	43.45	51.7	Ti	26.31	32.54	Ta	27.97	30.09
N	42.8	48.3	Al	19.92	21.39	Al	18.46	21.58
O	13.75	–	N	38.41	46.07	N	39.49	47.33
–		–	O	15.36	–	O	14.08	–

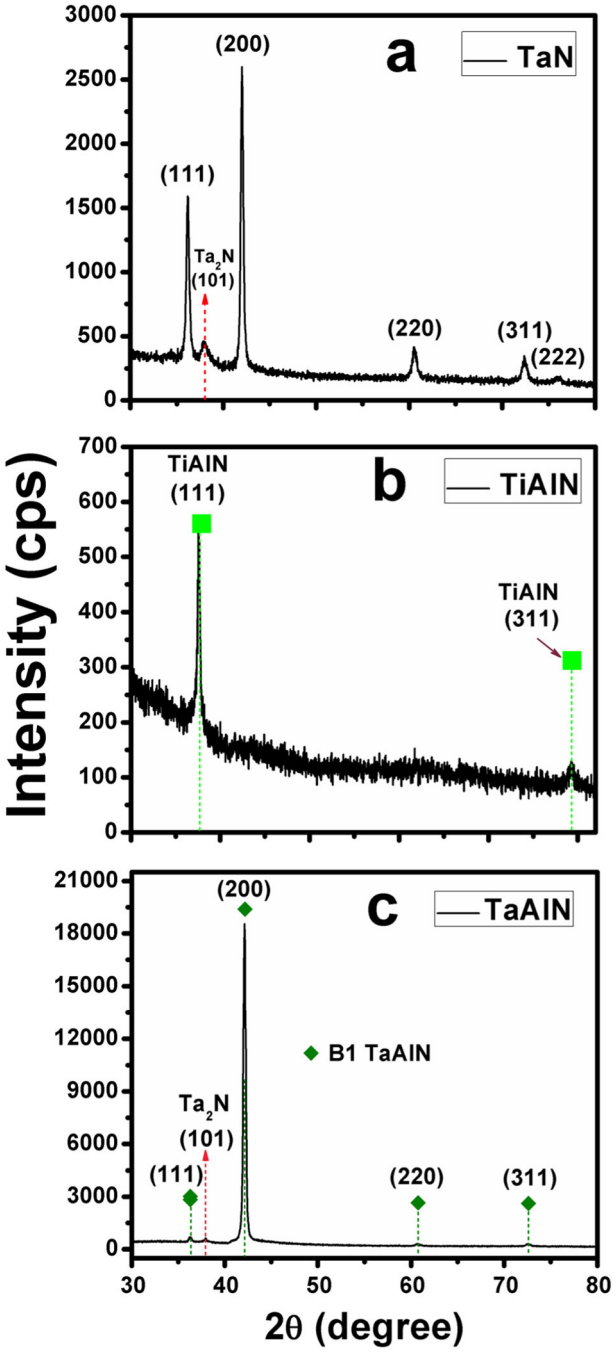

Fig. 4. XRD pattern of (a) TaN, (b) TiAlN, and (c) TaAlN coatings.

minimal lattice distortions (Fig. 4c). When sufficient thermal energy is available during coating formation, the texture changes from (111) orientation which is observed in the case of B1 TaAlN coatings. Elangovan et al. [42] observed a similar texture change in TaN coatings deposited through pulsed DC magnetron sputtering technique. The observed peaks at 36.3°, 60.7° and 72.6° could be attributed to (111), (220) and (311) planes of cubic B1 TaAlN structure. The XRD pattern of B1 TaAlN is well-matched with the previously reported results of TaAlN coating by Mikula et al. [17]. The calculated lattice parameter of the cubic TaAlN is found to be 4.308 Å. Also, a small volume fraction of Ta_2N phase was observed at 37.9° due to thermal stress associated with the coating after deposition [43]. The estimated average crystallite size of TaN, TiAlN and TaAlN coatings using Scherrer equation is found to be 17 nm, 16 nm and 21 nm, respectively.

The surface morphologies as well as cross-sectional view of all the coatings were observed using FE-SEM and the resulting images are illustrated in Fig. 5a-c. The grains are agglomerated and forming the particles with the size between 50 and 200 nm for TaN coating (Fig. 5a). These particles are originated from the Ta seeding layer and forming the columnar growth with spherical topped particles. Such columnar structure is well-established in the cross-sectional FE-SEM image (Fig. 5a). The similar morphology and growth pattern is obtained for the TaAlN coating. However, the columnar growth is discontinuous due to the incorporation of Al into the TaN phase (Fig. 5c). Therefore, the size of the particles also decreased to 20–150 nm for TaAlN coating (Fig. 5c). In comparison, highly-dense packed cross-sectional morphology is obtained for the TaAlN coatings. In the case of TiAlN coating, the typical triangular shaped particles with the size of ~40 nm (Fig. 5b) and the columnar growth pattern is formed across the coating thickness. All the deposited films are in the thickness ranges of 1.4–1.7 μm (Fig. 5a–c). In comparison, AFM topography also indicated the uniform distribution of particle size (Fig. 5d–f). The surfaces are relatively smooth for all the samples with the average root mean square (RMS) roughness values of 15 nm, 3 nm and 8 nm corresponding to the TaN, TiAlN and TaAlN samples, respectively. This smoother surface might be due to the lower surface energy and higher kinetic energy of adsorbed adatoms and leads to lower nucleation barrier during the sputter depositions [44]. Quantitative chemical composition analysis of all the coatings is carried out on the cross-section using EDAX and the results are provided in Table 1 and Fig. S2. It is clear that the primary elements are present in all the respective samples. Unlike XPS spectra (Figs. 1–3), O atoms have not been observed from the EDAX results as these analyses were carried across the coatings. This result revealed that the oxygen impurities were predominantly adsorbed from the atmosphere during the post-deposition exposure of samples resulting in surface oxides formation.

3.3. Tribological properties

The tribological properties of all the three samples are tested in humid-atmospheric and high-vacuum conditions to evaluate the comprehensive analysis of oxidative wear behavior using ball-on-disc tribometer.

3.3.1. Frictional and wear characteristics of coatings under humid-atmospheric and high-vacuum conditions

Tribological tests were conducted under humid-atmospheric and high-vacuum conditions to analyze the tribochemistry of the as-deposited coatings. The resulting friction curves are illustrated in Fig. S3 and the average friction coefficient values with error deviation are shown in Fig. 6. The FE-SEM wear micrographs of each sample tested in both conditions are illustrated in Fig. S4. The friction value is relatively lower for TaN in humid-atmospheric condition (~0.15), whereas it is higher (~0.38) in high-vacuum condition (Fig. 6a). The oxidized wear particles of both sliding bodies forms the lubricious layer (Figure S4a_1) followed by less friction in the ambient atmosphere (Fig. 6a). It is a well-known fact that the abrasive wear dominates in the metal-oxides, and hence, severe wear took place resulting higher wear rate of 1.7×10^{-4} mm^3/Nm (Fig. 6b) [45]. In contrast, severely deformed wear morphology is obtained in high-vacuum condition (Figure S4a_2) and there is no trace of wear particles attachment on the sample. It is anticipated that the wear particles could be continuously removed due to high-vacuum pumping and new surfaces simultaneously interact with each other and causing higher wear. Therefore, the calculated wear rate was comparably higher (3.1×10^{-4} mm^3/Nm) for TaN sample tested in high-vacuum condition (Fig. 6b). The higher wear rate is obtained because of its larger columnar grain structure of TaN coating (Fig. 5a) would limit the resistance to plastic deformation. The wear profile in Fig. S5a clearly evidenced that the wear depth reached the total coating thickness of ~1.5 μm in both the sliding tests.

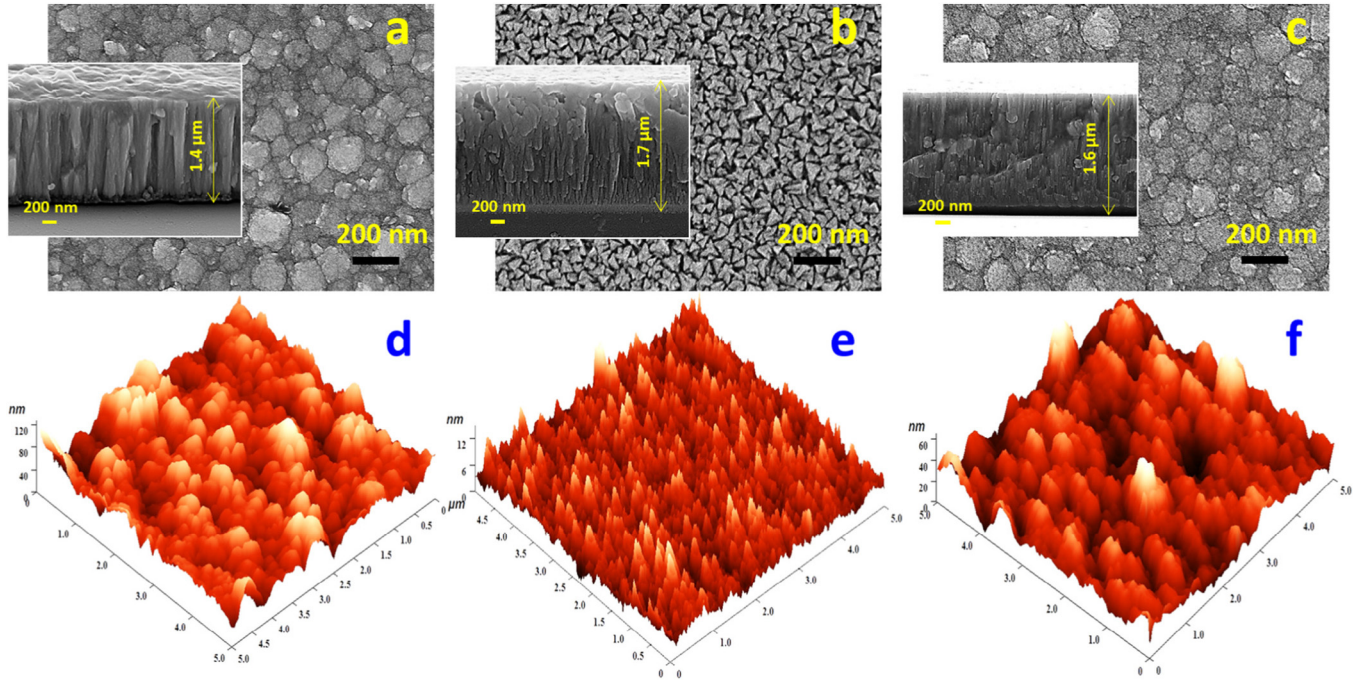

Fig. 5. Surface morphologies and topographies of (a & d) TaN, (b & e) TiAlN and (c & f) TaAlN coatings. [Inset image: Cross-sectional FE-SEM images of (a) TaN, (b) TiAlN, and (c) TaAlN coatings].

The friction value of TiAlN coating is found to be lower (~0.15) in the ambient condition and increased (~0.38) in the vacuum condition. The higher value of friction observed in the vacuum condition could be due to the severe abrasive wear behavior and poor crystalline nature of this coating. Highly deformed wear and large contact area (Figure S4b_1 and S4b_2) are clearly evidenced from the formation of the transfer layer from ball to the coating followed by the steel-steel sliding interfaces which result in higher friction [46]. For TaAlN coating, the addition of Al in TaN phase (TaAlN coating) produces lower average friction of 0.25 in ambient condition (Fig. 6a). Herein, Al substitutes Ta atoms in the cubic TaN lattice which would enhance the strength against deformations and oxidation resulting in superior wear resistance in atmospheric tribology test (4.7×10^{-8} mm^3/Nm). The XRD result (Fig. 4c) indicated well-defined B1 cubic structure of TaAlN phase majorly attained in the coating with highly dense microstructure lead to the higher resistance to the plastic deformation. Moreover, the improved properties also anticipated due to the formation of preferential growth of crystals along (200) plane which is in good agreement with the recent report on TaN coatings by Tan et al. [47]. Interestingly, the lowest friction coefficient (0.27) is obtained for TaAlN coating as compared to the TaN and TiAlN coatings tested in high-vacuum condition (Fig. 6b). There are several micro scratches obtained in the wear morphology (Fig. S4c_1) in the atmospheric test. However, this coating shows high wear resistance with the wear rate of 1.9×10^{-8} mm^3/Nm (Fig. 6b).

3.3.2. Tribochemical analysis of wear tracks

3.3.2.1. XPS and EDAX analysis. To further investigate the chemical bonding and to understand the friction and wear behavior with respect to the change in tribology conditions, sliding surfaces of all the samples were analyzed using XPS and EDAX techniques. The EDAX spectra and quantitative chemical composition results of all the tested samples are shown in Figs. S6–S9 and Table S1, respectively. The XPS survey spectrum of all the tests is shown in Fig. S10 and the quantitative composition results are given in Table S1. Fig. 7a-d illustrates deconvoluted high-resolution Ta 4f, N 1s, Fe 2p and O 1s spectra of TaN coating tested in atmospheric and vacuum conditions. Under the atmospheric sliding condition, the chemical compositions of Ta (20.33 at.%), N (18.79 at.%), Fe (12.67 at.%) and O (35.85 at.%) were observed by using XPS for the TaN coating (Table S1). The tribolayer consists of similar chemical compositions due to the excessive wear behavior of TaN coating in both sliding conditions. The slight shift in

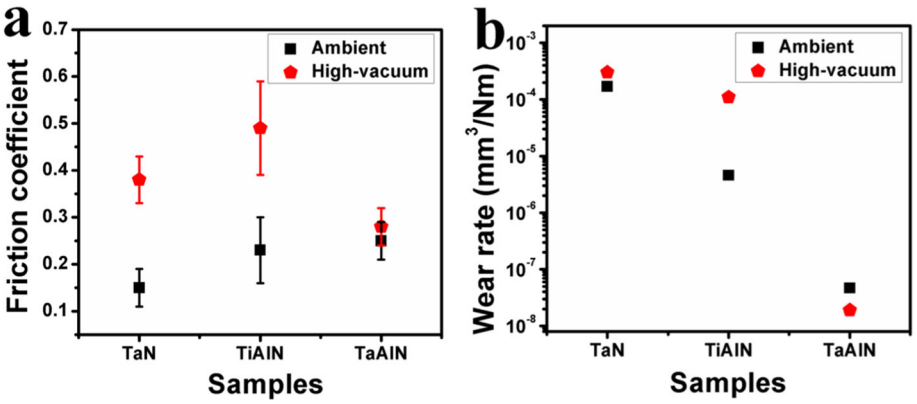

Fig. 6. (a) Average friction coefficient with error deviation of TaN, TiAlN, and TaAlN coatings in humid-atmospheric and high-vacuum sliding conditions and (b) Calculated wear rate of TaN, TiAlN, and TaAlN coatings in humid-atmospheric and high-vacuum sliding conditions. Tribology parameters: load: 1 N, sliding speed: 100 rpm (linear speed: 1.04 cm/s), sliding distance: 100 m, ball: 100Cr6 steel (dia. 6 mm).

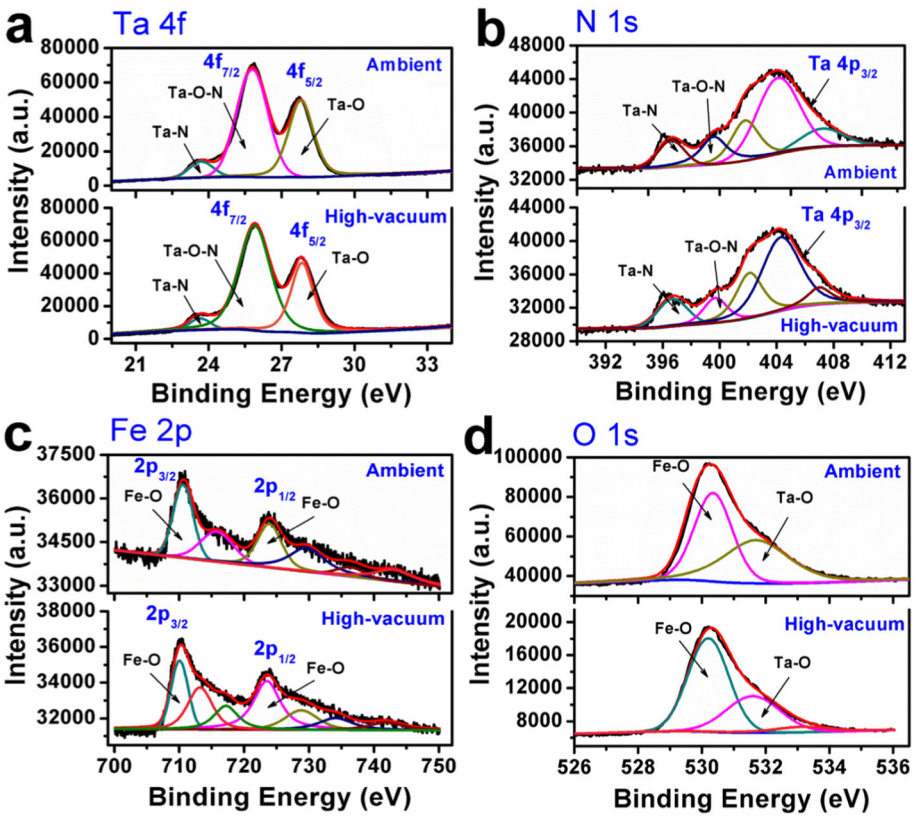

Fig. 7. High-resolution XPS spectra of TaN coating wear track after the tribological tests under (a) humid-atmospheric and (b) high-vacuum conditions. The figure comprises of Ta 4f, N 1s, Fe 2p, and O 1s spectra of TaN coating tested in both the conditions. Tribology parameters: load: 1 N, sliding speed: 100 rpm (linear speed: 1.04 cm/s), sliding distance: 100 m, ball: 100Cr6 steel (dia. 6 mm).

higher binding energies (~0.2 eV) of doublets $4f_{7/2}$ and $4f_{5/2}$ (Ta−N (23.5 eV), Ta−O−N (25.6 eV) and Ta−O (27.2 eV)) compared to the surface (Fig. 1) signifies the influence of oxygen with Ta during the tribology test and post-exposure of atmosphere [29,43]. Two peaks of Ta−N (396.4 eV) and Ta−O−N (399.8 eV) are obtained with lower intensity as seen in N 1s spectra (Fig. 7b) due to the higher wear loss in the sample in both conditions. Moreover, the obtained strong peaks in Fig. 7c implies the formations of FeO (710 eV) and Fe_2O_3 (724.1 eV) phases on both the wear track [48,49]. Herein, the additional shakeup peaks in Fe 2p spectra attributed to the satellite peaks of their respective primary peaks. According to the EDAX elemental mapping results, the oxidation is predominant on the ambient test sample as revealed from the binding energies of 530.2 eV and 531.9 eV corresponding to the FeO and Ta_2O_5 phases (Fig. 7d). The EDAX analysis (Fig. S6a) of atmospheric condition depicts the chemical composition of Ta (28.35 at.%) and N (24.65 at.%) elements which dominated inside the wear track with the other major elements Fe (4.2 at.%) and O (38.87 at.%) (Table S1). Wear particles were removed by the vacuum and exposure of substrate certainly took place in the high-vacuum sliding condition which representing the higher concentration of Fe (53.66 at.%) and Cr (17.2 at.%) than the coating elements Ta (11.05 at.%) and N (7.36 at.%). Similarly, the elements of Ta, N and Fe were observed with their respective concentrations of 21.91 at.%, 19.52 at.% and 47.94 at.% from the XPS results (Table S1) for TaN coating tested in vacuum condition.

The core level XPS spectra of TiAlN worn surface divulge the simultaneous formation of Ti and Al oxides (Fig. 8a and b). The Ti 2p doublets ($2p_{5/2}$ and $2p_{3/2}$) are shifted to the higher binding energies as compared to the TiAlN surface and the fitted peaks are resembling the Ti−O−N (456.7 eV) and Ti−O (458.1 eV) [30,33]. The EDAX results (Fig. S7a) also indicates the Fe predominant (22.73 at.%) than the coating elements (Ti-2.19 at.%, Al-5.33 at.% and N-7.53 at.%) along with the predominant O concentration about 40.16 at.%. Therefore, the oxidation of Al components is predominant on the wear surface with the obtained binding energies of 73.1 eV and 75 eV which is attributed to the Al−O−N and Al−O bonding, respectively. This is due to the removal of titanium oxides from the worn surface with excessive abrasive wear behavior [50]. N1s spectra (Fig. 8c) revealed the Al−O−N (398.2 eV) bonding formation in ambient condition, whereas, the Ti−Al−N (396.5 eV) and Al−O−N (398.1 eV) phases are co-existing in vacuum test. The absence of passivating media, less crystallinity, and high contact stress lead to high friction as well as severe wear behavior of TiAlN coating tested in vacuum conditions [51]. Moreover, it is revealed from the Fig. 8d (Fe 2p spectra), frequent transfer layers from ball to the coating surface resulting steel-steel sliding interactions leading to the higher wear and friction in both tribological conditions. The resultant higher oxidation of Fe and Al in the ambient condition is further confirmed from the deconvoluted O 1s spectra (Fig. 8e). In this condition, the composition results in Table S1 designate the presence of predominant O (37.92 at.%) along with the Fe (29.83 at.%) and Al (6.81 at.%) on the wear track. The EDAX mapping result (Fig. S7b) divulge the predominant existence of Fe (40.88 at.%) in vacuum test, however, the profilometer result (Fig. S5b) discloses the lower wear depth as compared to the coating thickness. This might be due to the higher wear particles from sliding counter body (i.e. SS ball) were intermixed and forming a solid solution passivation layer during the sliding test [52]. The existing surface metal atoms on the wear tracks are highly active to the oxidation immediately exposed to the atmosphere and thus the resulting spectra of vacuum tested samples exhibited with the fingerprints Ti−O, Al−O and Fe−O bonding corresponding to the TiO_2, Al_2O_3 and FeO/Fe_2O_3 phases, respectively. The corresponding EDAX and XPS chemical compositions results of TiAlN coating tested in high-vacuum condition are furnished in Table S1. The deconvoluted XPS core-level spectrum in Fig. 9 depicts the chemical products and their bonding nature of TaAlN coating worn surface in both sliding conditions. The doublets of $4f_{7/2}$ and $4f_{5/2}$ in Ta 4f (Fig. 9a) spectra of the sample tested in humid-atmospheric condition can be fitted into several binding energies corresponding to the covalent bonding of Ta−N (23.7 eV), Ta−Al−N (25.4 eV) and Ta−O−N (27.2 eV) formation. The chemical compositions of Ta (14.21 at.%), Al (8.91 at.

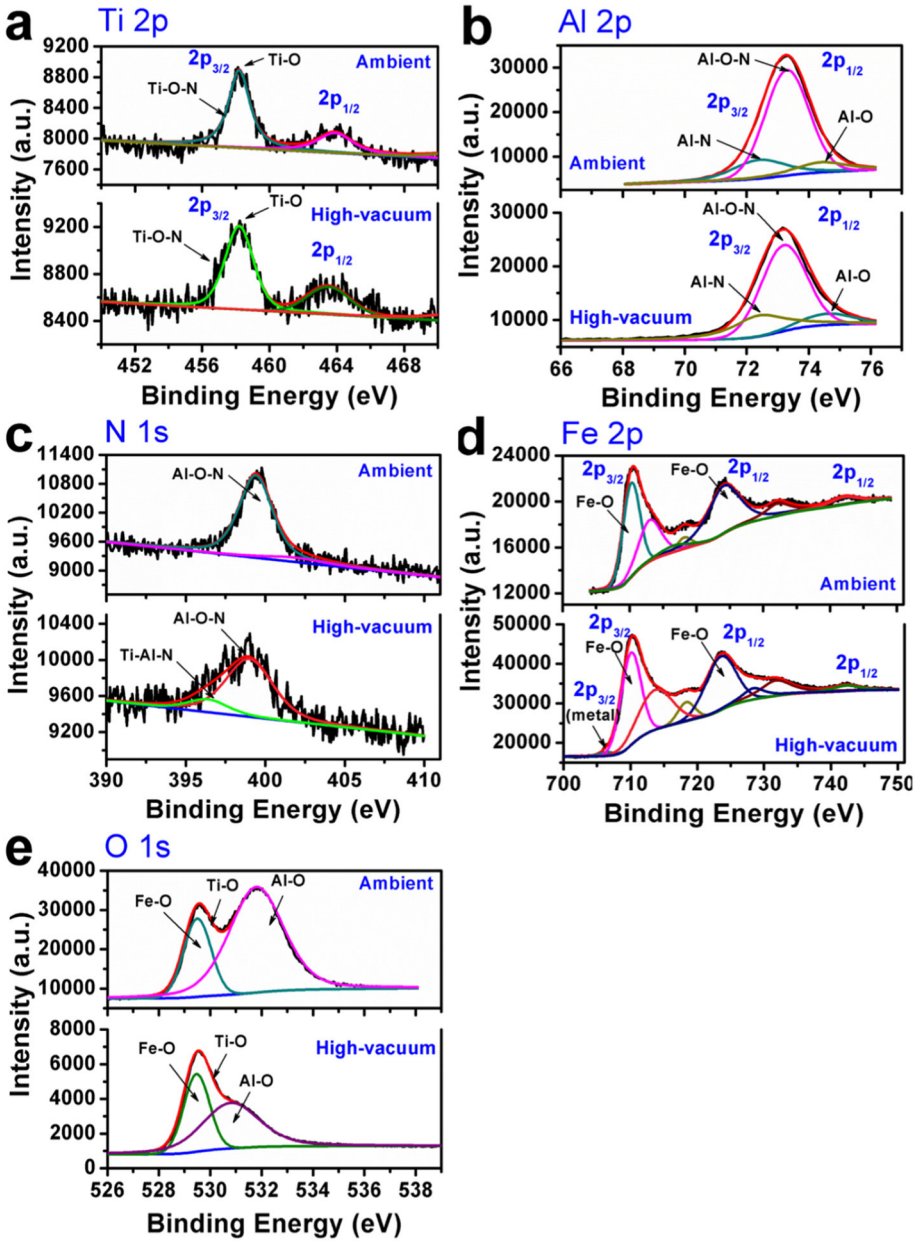

Fig. 8. High-resolution XPS spectra of TiAlN coating wear track after the tribological tests under (a) humid-atmospheric and (b) high-vacuum conditions. The figure comprises of Ti 2p, Al 2p, N 1s, Fe 2p, and O 1s spectra of TiAlN coating tested in both the conditions. Tribology parameters: load: 1 N, sliding speed: 100 rpm (linear speed: 1.04 cm/s), sliding distance: 100 m, ball: 100Cr6 steel (dia. 6 mm).

%), N (5.77 at.%), Fe (20.4 at.%) and O (40.44 at.%) were obtained from the XPS results (Table S1). In addition, obtained strong peak at 21.7 eV attributed to the metallic Ta, and it is due to the Ta ions formation during the tribo-oxidation mechanism [22]. Less oxidation of Ta in the worn surface is due to the enrichment of aluminum oxide (Al_2O_3) and iron oxide (FeO/Fe_2O_3) phases in the tribolayer as ascribed from the Al 2p and Fe 2p spectra (Fig. 9b and d). In these spectra, Al_2O_3 and Fe_2O_3 phases were identified from the resultant binding energies of 76.9 eV, 710 eV and 724.1 eV [47]. Such extreme surface oxidation could be further confirmed from predominant peaks of 529.2 eV (Fe—O) and 531.7 eV (Al—O) in the O 1s spectra (Fig. 9e). Because of the excessive surface oxidation, the N 1s spectrum illustrates the bonding formation of Ta—O—N at 398.2 eV (Fig. 9c). The wear track comprises of predominant oxygen concentration (50.64 at.%) along with the Fe (8.6 at.%), Al (10.45 at.%) and Ta (10.29 at.%) as provided in Table S1. It can be seen that the Fe, Al, and O are coexisting across the wear track which might be formed a strong passivation metal oxide (Fe—O and Al_2O_3) layers resulting lower friction coefficient of TaAlN coating [52]. Interestingly, the phase stability of TaAlN is significant for the tribo-test carried out in vacuum conditions. The observed results from Ta 4f, N 1s and Al 2p in Fig. 9 clearly indicated the similar chemical bonding formation compared to the surface (Fig. 3). The chemical states of Fe based components are significantly lower (Fig. 9d) and this result is in agreement with the EDAX elemental mapping (Fig. S8b). Composition results (Table S1) for the TaAlN coating tested in high-vacuum condition also revealed that the lower concentration of Fe (7.25 at.%) and O (4.08 at.%) along with the major compositions of Ta (34.21 at.%), Al (20.77 at.%) and N (33.04 at.%). It is suggested that the oscillated friction curve under vacuum conditions could be the possible frequent strain hardening of tribolayer under highly stressed sliding conditions. The above results concluding that the TaAlN coating possesses yield an extremely stable phase with improved friction and wear resistance

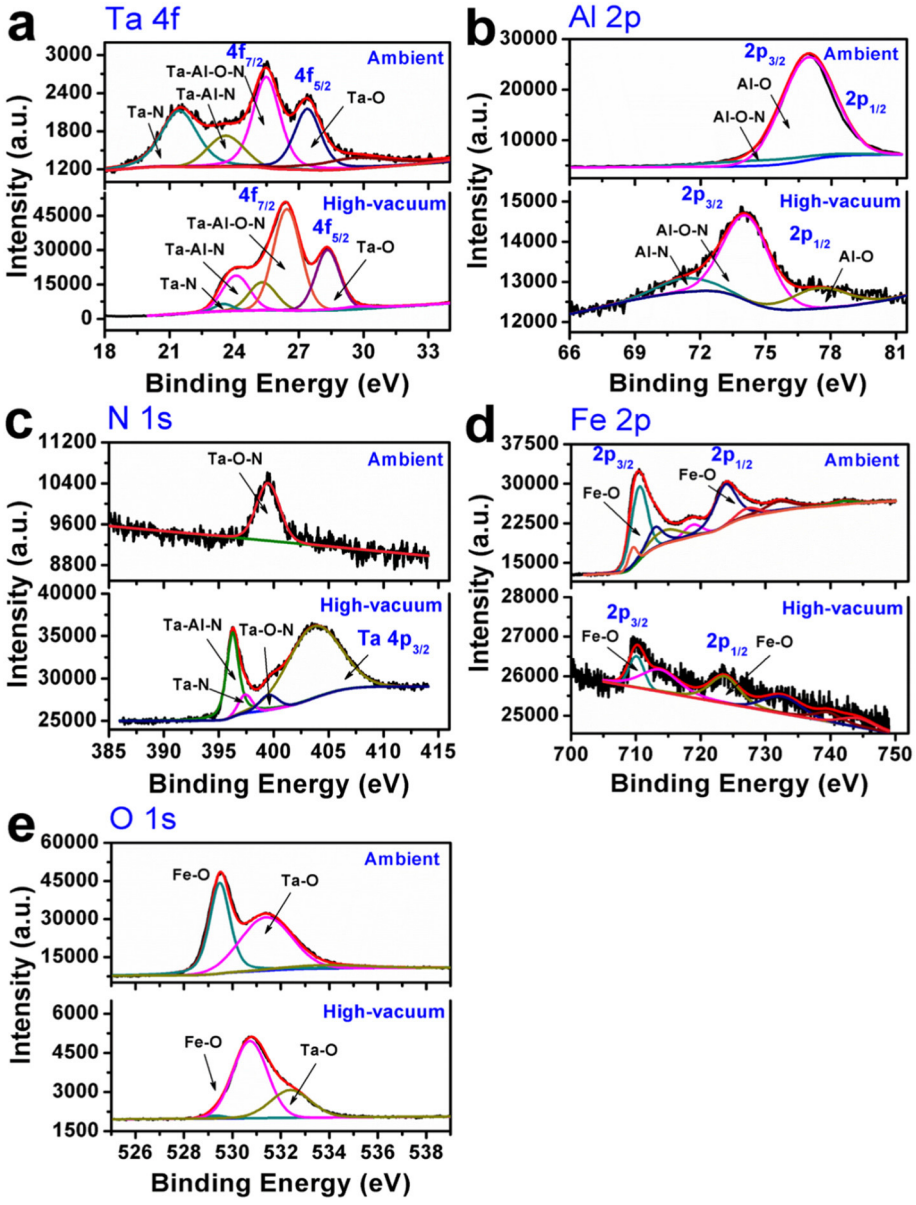

Fig. 9. High-resolution XPS spectra of TaAlN coating wear track after the tribological tests under (a) humid-atmospheric and (b) high-vacuum conditions. The figure comprises of Ta 4f, Al 2p, N 1s, Fe 2p, and O 1s spectra of TaAlN coating tested in both the conditions. Tribology parameters: load: 1 N, sliding speed: 100 rpm (linear speed: 1.04 cm/s), sliding distance: 100 m, ball: 100Cr6 steel (dia. 6 mm).

behavior at the selected tribological conditions.

4. Conclusions

The TaN, TiAlN and TaAlN coatings were deposited on 316LN SS substrates by reactive DC magnetron sputtering technique under optimized process conditions. Chemical bonding and crystallography results revealed the covalent bonding and formation of the well-defined cubic crystal structure for TaN, TiAlN and TaAlN coatings. The excessive tribochemical oxidative products such as Ta_2O_5, TiO_2, Al_2O_3, and FeO/Fe_2O_3 were formed in tribo-interfaces between TaN and TiAlN coatings and steel balls led to less friction (0.15–0.3) in ambient atmospheric tribo-condition, however, higher abrasive wear loss occurred. The larger columnar microstructure of TaN, lower crystalline nature of TiAlN and absence of passivating oxide tribolayer would decrease the resistance to plastic deformation and result in the higher wear loss of TaN and TiAlN coatings in high-vacuum sliding conditions. Large coverage of Al_2O_3 rich passivating tribolayer across the sliding interfaces between TaAlN coating and steel ball resulted in low friction (0.25) and high wear resistance behavior in ambient atmospheric tribo-condition. Even in the absence of passivating media, the TaAlN coating was quite stable and exhibited with low friction (0.27) and superior wear resistance in high-vacuum condition. The strong solid solution formation of Al into the TaN lattice and (200) preferred crystal orientation with higher crystallinity enhanced the tribological properties of TaAlN coating. Therefore, it is suggested that the TaAlN coating can be an ideal candidate for improved tribological performance irrespective of the tribological conditions.

Acknowledgments

D. Dinesh Kumar gratefully acknowledges the Department of Science and Technology-Science and Engineering Research Board (DST-SERB), Government of India, for providing financial support to carry out the research work under the Core Research Grant scheme (Sanction order number: CRG/2018/001448).

Appendix A. Supplementary data

Supplementary data to this article can be found online at https://doi.org/10.1016/j.apsusc.2019.143989.

References

[1] A.V. Bondarev, D.G. Kvashnin, I.V. Shchetinin, D.V. Shtansky, Temperature-dependent structural transformation and friction behavior of nanocomposite VCN-(ag) coatings, Mater. Des. 160 (2018) 964–973.
[2] Z. Li, Y. Wang, X. Cheng, Z. Zeng, J. Li, X. Lu, L. Wang, Q. Xue, Continuously growing Ultrathick CrN coating to achieve high load-bearing capacity and good Tribological property, ACS Appl. Mater. Interfaces 10 (2018) 2965–2975.
[3] A. Pogrebnjak, K. Smyrnova, O. Bondar, A. Pogrebnjak, K. Smyrnova, O. Bondar, Nanocomposite multilayer binary nitride coatings based on transition and refractory metals: structure and properties, Coatings 9 (2019) 155.
[4] K.V. Smyrnova, A.D. Pogrebnjak, V.M. Beresnev, S.V. Litovchenko, S.O. Borba-Pogrebnjak, A.S. Manokhin, S.A. Klimenko, B. Zhollybekov, A.I. Kupchishin, Y.O. Kravchenko, O.V. Bondar, Microstructure and physical–mechanical properties of (TiAlSiY)N nanostructured coatings under different energy conditions, Met. Mater. Int. 24 (2018) 1024–1035.
[5] Z. Li, P. Munroe, Z. Jiang, X. Zhao, J. Xu, Z. Zhou, J. Jiang, F. Fang, Z. Xie, Designing superhard, self-toughening CrAlN coatings through grain boundary engineering, Acta Mater. 60 (2012) 5735–5744.
[6] A.Z. Ait-Djafer, N. Saoula, H. Aknouche, B. Guedouar, N. Madaoui, Deposition and characterization of titanium aluminum nitride coatings prepared by RF magnetron sputtering, Appl. Surf. Sci. 350 (2015) 6–9.
[7] J.Y. Yi, K.H. Chen, Y.C. Xu, C.J. Zhu, Performance of AlTiBN and AlTiTaN coatings during milling of titanium, Surf. Eng. 35 (2019) 501–506.
[8] L. Chen, Y.X. Xu, Influence of interfacial structure on the mechanical and thermal properties of CrAlN/ZrN multilayer coatings, Mater. Des. 106 (2016) 1–5.
[9] M. Roy, Protective hard coatings for Tribological applications, Mater. Under Extrem. Cond, Elsevier, 2017, pp. 259–292.
[10] X. Guo, Y. Niu, M. Chen, W. Sun, S. Zhu, F. Wang, Stoichiometry and tribological behavior of thick ta(N) coatings produced by direct current magnetron sputtering (DCMS), Appl. Surf. Sci. 427 (2018) 1071–1079.
[11] A.D. Pogrebnjak, Y.O. Kravchenko, O.V. Bondar, B. Zhollybekov, A.I. Kupchishin, Structural features and Tribological properties of multilayer coatings based on refractory metals, Prot. Met. Phys. Chem. Surfaces. 54 (2018) 240–258.
[12] V. Khetan, N. Valle, D. Duday, C. Michotte, C. Mitterer, M.-P. Delplancke-Ogletree, P. Choquet, Temperature-dependent Wear mechanisms for magnetron-sputtered AlTiTaN hard coatings, ACS Appl. Mater. Interfaces 6 (2014) 15403–15411.
[13] M. Pfeiler, G.A. Fontalvo, J. Wagner, K. Kutschej, M. Penoy, C. Michotte, C. Mitterer, M. Kathrein, Arc evaporation of Ti–Al–ta–N coatings: the effect of Bias voltage and ta on high-temperature Tribological properties, Tribol. Lett. 30 (2008) 91–97.
[14] V. Khetan, N. Valle, D. Duday, C. Michotte, M.-P. Delplancke-Ogletree, P. Choquet, Influence of temperature on oxidation mechanisms of fiber-textured AlTiTaN coatings, ACS Appl. Mater. Interfaces 6 (2014) 4115–4125.
[15] Y.-I. Chen, J.-H. Lin, C.-C. Chou, Oxidation resistance and mechanical properties of ta–Al–N coatings, Surf. Coatings Technol. 303 (2016) 41–47.
[16] C.M. Koller, R. Hollerweger, R. Rachbauer, S. Kolozsvári, J. Paulitsch, P.H. Mayrhofer, Annealing studies and oxidation tests of a hybrid multilayer arrangement of cathodic arc evaporated Ti–Al–N and reactively sputtered ta–Al–N coatings, Surf. Coatings Technol. 283 (2015) 89–95.
[17] M. Mikula, D.G. Sangiovanni, D. Plašienka, T. Roch, M. Čaplovičová, M. Truchlý, L. Satrapinskyy, R. Bystrický, D. Tonhauzerová, D. Vlčková, P. Kúš, Thermally induced age hardening in tough ta-Al-N coatings via spinodal decomposition, J. Appl. Phys. 121 (2017) 155304.
[18] N. Schalk, T. Weirather, C. Sabitzer, S. Hirn, V.L. Terziyska, S. Gangopadhyay, C. Czettl, P. Polcik, M. Kathrein, C. Mitterer, Combinatorial synthesis of Cr1 − xAlxN and Ta1 − xAlxN coatings using industrial scale co-sputtering, Surf. Eng. 32 (2016) 252–257.
[19] J. Hao, Y. Zhang, P. Ren, K. Zhang, J. Chen, S. Du, M. Wang, M. Wen, Spinodal decomposition in the ta-Mo-Al-N films activated by Mo incorporation: toward enhanced hardness and toughness, Ceram. Int. 44 (2018) 21358–21364.
[20] S.M. Hsu, J. Zhang, Z. Yin, The nature and origin of Tribochemistry, Tribol. Lett. 13 (2002) 131–139.
[21] J.L. Mo, M.H. Zhu, Tribological oxidation behaviour of PVD hard coatings, Tribol. Int. 42 (2009) 1758–1764.
[22] A. Zaman, E. Meletis, Microstructure and mechanical properties of TaN thin films prepared by reactive magnetron sputtering, Coatings 7 (2017) 209.
[23] K. Bobzin, E. Lugscheider, R. Nickel, N. Bagcivan, A. Krämer, Wear behavior of Cr1 − xAlxN PVD-coatings in dry running conditions, Wear 263 (2007) 1274–1280.
[24] R.C. Dante, C.K. Kajdas, A review and a fundamental theory of silicon nitride tribochemistry, Wear 288 (2012) 27–38.
[25] S. Du, K. Zhang, Q. Meng, P. Ren, C. Hu, M. Wen, W. Zheng, N dependent tribochemistry: achieving superhard wear-resistant low-friction TaCxNy films, Surf. Coatings Technol. 328 (2017) 378–389.
[26] J. Ma, X. Qi, Y. Dong, Y. Zhao, Q. Zhang, B. Fan, Y. Yang, Transfer film formation mechanism and tribochemistry evolution of a low-wear polyimide/mesoporous silica nanocomposite in dry sliding against bearing steel, Tribol. Int. 120 (2018) 233–242.
[27] S. Wan, A.K. Tieu, Y. Xia, L. Wang, D. Li, G. Zhang, H. Zhu, B.H. Tran, D.R.G. Mitchell, Tribochemistry of adaptive integrated interfaces at boundary lubricated contacts, Sci. Rep. 7 (2017) 9935.
[28] Y. Zhou, D.N. Leonard, H.M. Meyer, H. Luo, J. Qu, Does the use of diamond-like carbon coating and organophosphate lubricant additive together cause excessive Tribochemical material removal? Adv. Mater. Interfaces 2 (2015) 1500213.
[29] X. Yang, E. Aydin, H. Xu, J. Kang, M. Hedhili, W. Liu, Y. Wan, J. Peng, C. Samundsett, A. Cuevas, S. De Wolf, Tantalum nitride Electron-selective contact for crystalline silicon solar cells, Adv. Energy Mater. 8 (2018) 1800608.
[30] M. de Respinis, M. Fravventura, F.F. Abdi, H. Schreuders, T.J. Savenije, W.A. Smith, B. Dam, R. van de Krol, Oxynitrogenography: controlled synthesis of single-phase tantalum Oxynitride Photoabsorbers, Chem. Mater. 27 (2015) 7091–7099.
[31] Y.K. Wang, W.M. Wang, X.H. Cu, X.Y. Cheng, B.S. Li, L.F. Xia, T.Q. Lei, A study of the oxide layer on the surface of a TiN coating, Mater. Chem. Phys. 36 (1993) 80–83.
[32] A. Rizzo, L. Mirenghi, M. Massaro, U. Galietti, L. Capodieci, R. Terzi, L. Tapfer, D. Valerini, Improved properties of TiAlN coatings through the multilayer structure, Surf. Coatings Technol. 235 (2013) 475–483.
[33] A. Esguerra-Arce, J. Esguerra-Arce, L. Yate, C. Amaya, L.E. Coy, Y. Aguilar, O. Gutiérrez, S. Moya, Influence of the Al content on the in vitro bioactivity and biocompatibility of PVD Ti1 − xAlxN coatings for orthopaedic applications, RSC Adv. 6 (2016) 60756–60764.
[34] M. Alishahi, F. Mahboubi, S.M. Mousavi Khoie, M. Aparicio, E. Lopez-Elvira, J. Méndez, R. Gago, Structural properties and corrosion resistance of tantalum nitride coatings produced by reactive DC magnetron sputtering, RSC Adv. 6 (2016) 89061–89072.
[35] C. Ozgit-Akgun, E. Goldenberg, A.K. Okyay, N. Biyikli, Hollow cathode plasma-assisted atomic layer deposition of crystalline AlN, GaN and AlxGa1 − xN thin films at low temperatures, J. Mater. Chem. C 2 (2014) 2123–2136.
[36] Y. Zhang, Y. Zheng, Y. Li, L. Wang, Y. Bai, Q. Zhao, X. Xiong, Y. Cheng, Z. Tang, Y. Deng, S. Wei, Tantalum nitride-decorated titanium with enhanced resistance to microbiologically induced corrosion and mechanical property for dental application, PLoS One 10 (2015) e0130774.
[37] J. Pelleg, L.Z. Zevin, S. Lungo, N. Croitoru, Reactive-sputter-deposited TiN films on glass substrates, Thin Solid Films 197 (1991) 117–128.
[38] T.J.B. Holland, S.A.T. Redfern, Unit cell refinement from powder diffraction data: the use of regression diagnostics, Mineral. Mag. 61 (1997) 65–77.
[39] Kamalan Kirubaharan A.M., Kuppusami P., Dharini T., Thermal expansion studies of electron beam evaporated yttria films on Inconel-718 substrates, Surf. Coatings Technol. 354 (2018) 297–305.
[40] S. PalDey, S. Deevi, Single layer and multilayer wear resistant coatings of (Ti,Al)N: a review, Mater. Sci. Eng. A 342 (2003) 58–79.
[41] C.A. Davis, A simple model for the formation of compressive stress in thin films by ion bombardment, Thin Solid Films 226 (1993) 30–34.
[42] T. Elangovan, S. Murugeshan, D. Mangalaraj, P. Kuppusami, S. Khan, C. Sudha, V. Ganesan, R. Divakar, E. Mohandas, Synthesis and high temperature XRD studies of tantalum nitride thin films prepared by reactive pulsed dc magnetron sputtering, J. Alloys Compd. 509 (2011) 6400–6407.
[43] J. Xu, L. Liu, P. Munroe, Z.-H. Xie, Promoting bone-like apatite formation on titanium alloys through nanocrystalline tantalum nitride coatings, J. Mater. Chem. B 3 (2015) 4082–4094.
[44] D.D. Kumar, N. Kumar, K. Panda, A.M. Kamalan Kirubaharan, P. Kuppusami, Tribochemistry of contact interfaces of nanocrystalline molybdenum carbide films, Appl. Surf. Sci. 447 (2018) 677–686.
[45] M. Antonov, H. Afshari, J. Baronins, E. Adoberg, T. Raadik, I. Hussainova, The effect of temperature and sliding speed on friction and wear of Si3N4, Al2O3, and ZrO2 balls tested against AlCrN PVD coating, Tribol. Int. 118 (2018) 500–514.
[46] D.D. Kumar, N. Kumar, S. Kalaiselvam, S. Dash, R. Jayavel, Substrate effect on wear resistant transition metal nitride hard coatings: microstructure and tribo-mechanical properties, Ceram. Int. 41 (2015) 9849–9861.
[47] P. Tan, L. Fu, J. Teng, J. Zhu, W. Yang, D. Li, L. Zhou, Effect of texture on wear resistance of tantalum nitride film, Tribol. Int. 133 (2019) 126–135.
[48] C.R. Das, N. Kumar, S. Dash, P. Chandramohan, M.P. Srinivasan, S.K. Albert, A.K. Tyagi, A.K. Bhaduri, B. Raj, Evolution of Tribological properties of reactor-grade NiCr-B coating, Tribol. Lett. 44 (2011) 229–235.
[49] K. Kutschej, P.H. Mayrhofer, M. Kathrein, P. Polcik, C. Mitterer, Influence of oxide phase formation on the tribological behaviour of Ti-Al-V-N coatings, Surf. Coatings Technol. 200 (2005) 1731–1737.
[50] A.F. Yetim, Investigation of wear behavior of titanium oxide films, produced by anodic oxidation, on commercially pure titanium in vacuum conditions, Surf. Coatings Technol. 205 (2010) 1757–1763.
[51] D.D. Kumar, N. Kumar, S. Kalaiselvam, R. Thangappan, R. Jayavel, Film thickness effect and substrate dependent tribo-mechanical characteristics of titanium nitride films, Surfaces and Interfaces 12 (2018) 78–85.
[52] J. Nohava, P. Dessarzin, P. Karvankova, M. Morstein, Characterization of tribological behavior and wear mechanisms of novel oxynitride PVD coatings designed for applications at high temperatures, Tribol. Int. 81 (2015) 231–239.